# Rheology of methane hydrate slurries during their crystallization in a water in dodecane emulsion under flowing

Annie Fidel-Dufour, Frédéric Gruy, Jean-Michel Herri

▶ **To cite this version:**

Annie Fidel-Dufour, Frédéric Gruy, Jean-Michel Herri. Rheology of methane hydrate slurries during their crystallization in a water in dodecane emulsion under flowing. Chemical Engineering Science, 2006, 61 (2), pp.505-515. 10.1016/j.ces.2005.07.001 . emse-03763489

**HAL Id: emse-03763489**

**https://hal-emse.ccsd.cnrs.fr/emse-03763489**

Submitted on 29 Aug 2022

**HAL** is a multi-disciplinary open access archive for the deposit and dissemination of scientific research documents, whether they are published or not. The documents may come from teaching and research institutions in France or abroad, or from public or private research centers.

L'archive ouverte pluridisciplinaire **HAL**, est destinée au dépôt et à la diffusion de documents scientifiques de niveau recherche, publiés ou non, émanant des établissements d'enseignement et de recherche français ou étrangers, des laboratoires publics ou privés.

**Title**

# Rheology of methane hydrate slurries during their crystallisation in a water in dodecane emulsion under flowing.

**Authors**

Annie FIDEL-DUFOUR, Frédéric GRUY and Jean-Michel HERRI*

Ecole des Mines de Saint-Etienne, SPIN, 158 cours Fauriel, 42023 Saint-Etienne Cedex 2, France.

* Author to whom correspondence should be addressed. E-mail address : herri@emse.fr

**keywords :**

crystallization, agglomeration, multiphase flow, rheology, gas hydrates

**Abstract**

In this paper is presented a model of agglomeration of methane hydrate particles during transportation of a water in oil emulsion which circulates in a high pressure (10 MPa) flow loop reactor specially designed for this application. The originality of this set-ups consists in the fact that fluid flow is ensured via gas-lift effect and does not require any pump. Influences of an anti-agglomerant additive and of water content in range [7-18% vol] are studied in the flow conditions. In particular, fluid viscosity is measured in real time, then correlated to gas consumption and hydrate agglomeration.

## Introduction

Gas hydrate particles are crystals which can form from cold liquid water and hydrocarbon gas under pressure (Sloan, 1998). These conditions are encountered during oil transportation in deep sea pipelines. They can cause plugs and present now a major problem of flow insurance for the production of the very deep wells.

Different methods are used to prevent or to control gas hydrate crystallization. They are classified in different classes depending on their role, either in thermodynamic prevention or in kinetic control.

As far as the thermodynamic prevention is concerned, the essential objective is to maintain the fluid outside the condition of the gas hydrates formation. This can be done by thermal insulation of the pipelines in order to keep constant the natural high temperature of the fluid exiting the well head. This method requires an important capital cost. Another thermodynamic method consists in injecting additives which shift the equilibrium condition and allow the fluid to be cooled down to the sea temperature without meeting the hydrate formation conditions. For example, glycols can be used to this aim, however due to glycol quantity to inject and to re-treat, high operational cost are generated.

A recent way of investigation deals with the use of low dosage hydrate inhibitors (LDHI) which can act on the crystallization kinetics while delaying nucleation, modifying growth, or preventing agglomeration. The advantage of this approach is the poor quantity of additives to be used : about 1% mass of the water phase (see reviewing of Ramesh *et al*, 2002)

The nature of the kinetic additive effect is rarely well understood, mostly because of the difficulty to interpret microscopic events from observation at the macroscopic scale. Attempts to model gas hydrate crystallization have been achieved on simple systems (water plus gas), and simple geometry (batch stirred reactors) using particle sizers (Herri *et al*, 1999, Pic *et al*, 2001). Generalization to real systems (water in oil emulsion) and real geometry flowing has never been achieved, due to the complexity of the task. In the practise, qualification of additive efficiency on real fluids is performed experimentally, firstly at the laboratory scale on batch systems or mini loop systems (for a first screening), then at the pilot scale and finally at the field scale (for instance, see review of Sinquin *et al*, 2004). Procedures can considerably vary between the laboratories and do not ensure possibilities of comparison or fundamental understanding.

In the open literature, the only tentative to connect rheology, crystallization, oil chemistry and additive influence has been performed by Camargo *et al* (2001, 2002). In these works, the authors studied an asphaltenic crude oil which exhibits a natural anti agglomerant effect and they compared this behaviour to that of a condensate which needs synthetic additives to prevent agglomeration. The experimental analysis consisted of a rheological characterization after complete crystallization, first at the laboratory scale and then at the pilot scale.

The approach which is developed in this paper is inspired on the work of Camargo *et al* from which we retain in particular the viscosity model based on Mills approach (1985). Here, we have a special attention for early steps of the crystallization process during which particle formation consumes gas and modifies the fluid viscosity:

- Description of the new flow loop reactor in which the suspension is flowing without any pump or mechanical machine. The objective is to minimize the high shear stress encountered in classical pumps which can deeply modify the nature and the way of crystallisation. This section includes the modelling of the global behaviour of the apparatus.
- Experimental results concerning the rheology of water in dodecane emulsion before and after hydrate crystallization, in the presence of an anti-agglomerant additive.
- Modelling of emulsion crystallization and evolution of suspension rheology.
- Discussion and conclusion.

## Experimental methods

### *Experimental set-up*

The experimental set up (Figure 1) is a flow loop reactor simulating some of the conditions of the oil flow in deep sea pipelines : pressure in the range of [1-10 MPa] and temperature in the range of [0-10°C].

The different parts of this apparatus are :

- the flow section is a large streamer of 36.1 m long, 1.02 cm internal diameter and constant slope of 4°. The streamer is composed of 3 identical levels. Each level is composed of 2 long straight pipes of 4 m long, 2 short sections of 0.3 m long, and four elbows of 0.5 m radius. The pipes are maintained at constant temperature by means of 9 external cooling jackets of 1.5 m long built on the 1shell-and-1tube principle. On the three levels constituting the streamer, 7 temperature probes monitor the fluid temperature profile. A global pressure drop measurement is performed between the entry and the exit.
- A parallel one meter pipe of ¼ inch diameter is mounted on an elbow of the loop. It is temperature controlled down to –20°C and it acts as a cold point to initiate crystals nucleation.
- The exit of the flow section is connected to a gas lift riser (10.6 m long and 1.73 cm internal diameter) in which gas coming from a separator located at the top of the column is re-injected. The gas lift temperature is controlled using 3 heat exchangers of 2 m long. A differential pressure transmitter monitors the pressure drop along this section. A temperature probe is mounted at the exit of the gas lift. The gas lift ensures both the flow driving force and the gas absorption.
- The input of the flow section is connected to the descending pipe (downcomer) (8.3 m height, 9.1 m long and internal diameter of 1.73 cm, plus a section of 0.39 m in internal diameter of 1.02 cm) coming from the separator and transporting the fluid after gas separation. The downcomer pipe is equipped with two heat exchangers of 2 m long, a temperature probe and a pressure drop sensor. A Coriolis mass-flow-meter is mounted on the downcomer pipe (Micro Motion R050)
- The gas separator is a tube of 2 inches external diameter and 2 m height. The gas lift tube enter into it on an height of 1.5 m. The geyser exiting the gas lift column is

separated into its different phases : gas phase goes up whereas liquid and solid phases go down and enter the downcomer pipe. Gas is then flowed to a gas booster unit.

- The gas booster unit consists of two ballasts in which liquid water is flowing from one to the other and inversely. One of the ballast acts as a sucker (sucking gas from the top of the separator) and the other one as a pusher (pushing gas at the bottom of the gas lift riser).

Finally, this gas lift is able to move the emulsion or the suspension without any pump or mechanical system. The driving force is the pressure difference ΔP between the bottom parts of the gas lift riser and downcomer pipe.

***Modelling of the global behaviour of the flow loop***

The pressure drop in the different sections of the set-up can be divided into three parts :

$$\Delta P_i = \int \rho g dh + \Delta P^1 + \Delta P^2 \qquad [1]$$

The first part is due to the gravity effect. If density does not change along the flow (reasonable assumption everywhere except in the gas lift where gas absorption can occur), it is equal to $\rho g \Delta h$

Second term is the regular pressure drop due to energy dissipation by fluid. In the laminar zone and for a newtonian fluid. It is given by the Poiseuille's law :

$$\Delta P^i = \frac{128 \mu Q}{\pi D_i^4} L_i \qquad [2]$$

where $Q$ is the liquid flow rate.

$\Delta P^2$ part is the singular pressure drop due to energy dissipation by fluid on pipe perturbations (elbows, connecting elements…). In the laminar regime, we showed that this contribution is only 6% of the regular contribution in the streamer section. The streamer section presents the highest number of singularities. We propose to account for the contribution of the

singularities by defining an equivalent pipe length. On the other parts of the flow loop, we neglect this contribution.

The pressure balance (Figure 2) can be done on the streamer side, or on the (gas lift pipe plus descending pipe plus separator) side.

On the streamer side, we can write :

$$\Delta P^1 = \frac{128 \mu Q}{\pi D^4} L \qquad [3]$$

On the other side, the loop is composed of :

- a gas lift section of height $h_2$, length $L_2=h_2$, diameter $D_1$,
- a gas separator in which liquid level $h_4$ is measured. $\Delta P^1$ contribution is neglected due to a large internal diameter of 4 cm,
- a descending pipe of height $h_1$ composed of a first section of length $L_1$, diameter $D_1$, and a second section of length $L_c$, diameter $D$,
- an elbow connecting section between the exit of the streamer and the entry of the gas lift (height $h_3$, length $L_3$, diameter $D$).

The pressure balance gives :

$$\Delta P1 = \rho g\left(h_4 + h_1 + h - h_3\right) - \frac{128\,\mu Q L}{\pi}\left(\frac{L_1}{D_1^4} + \frac{L_3}{D^4} + \frac{L_C}{D^4}\right) - \Delta P_2 \qquad [4]$$

The gas lift pressure drop contribution $\Delta P_2$ can be divided into gravity contribution and flow contribution :

$$\Delta P_2 = \rho_{GL} g h_2 + \Delta P_2^1 \qquad [5]$$

Flow contribution $\Delta P_2^1$ contribution in the gas lift riser need a special treatment due to the presence of gas bubbles which modify deeply the nature of the flow. This modelling is done in the next part of the paper.

From equation [3], [4] and [5], we can write :

$$\Delta P=\left[\rho g\left(h_4+h_1+h-h_2-h_3\right)-g\left(\rho_{GL}-\rho\right)h_2-\Delta P_2^1\right]\frac{L}{D^4}\Bigg/\left(\frac{L}{D^4}+\frac{L_1}{D_1^4}+\frac{L_3}{D^4}+\frac{L_C}{D^4}\right) \qquad [6]$$

***Modelling of flowing in the gas lift riser***

In the riser the flow may show different patterns : bubbly, slug, churn or annular. The nature of the flow can be determined from a diagram ( $\rho_L U_L^2$, $\rho_G U_G^2$ ) where $U_G, U_L$ are respectively the superficial velocities for gas and liquid (Scott, 1963, Hewitt, 1969). In our experimental set-up, the flow has a slug flow pattern ( $\rho_L U_L^2$=15 , $\rho_G U_G^2$=3 with $U_G/\left(U_G+U_L\right)$=0.64 ). Slug flow pattern is observed in the case of small-diameter riser (<0.05m). The gas flows largely in a Taylor bubble which occupies most of the pipe's cross-sectional area. Between Taylor bubble and the wall, a thin liquid film flows downward. Successive Taylor bubbles are separated in the axial direction by liquid slugs that bridge the pipe and carry distributed bubbles.

Mechanistic models for vertical slug flow have been suggested by several investigators. In this work, the hydrodynamics and the parameters of slug flow in the riser are described by employing the model of Yun and Shen (2003), which is based on the assumptions of Barnea (1990), Sylvester (1987) and Zhang (1991). All details will be found in the work of Yun *et al*.(2003).

Modelling of Yun *et al* (2003) requires the knowledge of physical properties of dodecane-water-methane system :

Compressibility coefficient of methane gas follows the relation :

$Z = 0.994 - 0.0196P$ with $P$ in MPa

Equilibrium concentration is given by Henry's law :

$c_{eq} = HP$ with $H$=2.9 $10^{-4}$ mole.m$^{-3}$.Pa$^{-1}$.

Methane in dodecane molar fraction at equilibrium in the pressure range [6.5-7 Mpa] is equal to 0.307. Dodecane density is equal to 750 $kgm^{-3}$ and density of dodecane/methane solution is 675 $kgm^{-3}$ at saturation.

Surface tension of dodecane/methane system is taken equal to 0.025 $Jm^{-2}$.

***Flow loop modelling conclusion***

The particular modelling of the pressure drop $\Delta P_2^1$ in the gas lift combined to the regular pressure drops in the rest of the loop (equation [6]) shows that, for a Newtonian fluid flowing in laminar conditions, the geometric location of the measured or calculated points of the couple ($\Delta P$,$Q$) is independent on the viscosity of the fluid however only depends on the gas injection rate $Q_G$. To illustrate this behaviour, we present in figure (3) an abacus of the geometric location ($\Delta P$,$Q$) at constant viscosity and variable $Q_G$ (straight lines passing through origin), and constant $Q_G$ but variable viscosity (hyperbolic curves).

***Experimental protocol***

The experimental results which are presented in this paper are relative to the influence of additives on the rheology of the water in oil emulsion before crystallisation and of the hydrate suspension during crystallisation.

The system under study is composed of water, dodecane and an additive.

Water is tap water. Dodecane is 99.9 % pure dodecane from V3 CHIMIE. Methane is pure 99.99% from AIR LIQUIDE. The additive is an anti-agglomerant solution (IPE 202) patented by IFP (Institut Français du Pétrole).

The total volume of the solution is 7.9 L. The water mass fraction varies in the range [5-30%]. The additive is added in various proportions to stabilize the suspension during crystallisation.

The additive mass fraction varies in the range [0-0.5 %] of the oil mass. The emulsion is prepared in a batch reactor under stirring and then introduced in the loop.

After introduction, the flow is forced by air injection at the bottom of the gas lift. Once operating temperature reached [2-4°C], the rheological characterization of the emulsion can be performed by varying the air injection rate.

Then, air injection is stopped and the gas separator is connected to the ballasts of the gas booster unit. The system is filled with methane gas up to a pressure of 7 MPa (first pressurisation in Figure 4). The pump between the two ballasts of the gas booster unit is started and methane gas is injected at the bottom of the gas lift. Loop flow starts and pressure strongly decreases due to gas consumption in the gas lift. After 10 min, the gas injection is stopped and system is filled again up to 7 MPa. Gas injection is re-started and loop flow starts again. Total pressure decreases slightly and liquid saturation is reached. During this saturation phase, we can observe that temperature is not perfectly controlled (still maintained in the range [2-5°C]). The reason for is that the loop needs to flow to be normally cooled because the 14 heat exchangers ensures a heat insulation on only one half of the loop.

After a while (60 min in Figure 4), gas hydrate crystallisation occurs and a sudden temperature drop is detected in relation to a pressure decrease : crystallisation is exothermic and consumes methane gas which is incorporated in the hydrate phase. As a consequence of crystallisation, pressure finally reaches a plateau from which we can determine the water conversion into hydrates. Except during the first instants of crystallisation, temperature is correctly controlled in the range [2.5-3.5°C].

**Experimental results**

***Water in oil emulsion characterization***

In Figure 5 are plotted the experimental points ($Q,\Delta P$) for 7 % (volumic) water content in oil emulsion, at various additive concentration, temperature of 4 °C and pressure of 0.1 MPa. From this curve, we can clearly deduce that the water in oil emulsion presents a Newtonian behaviour. The additive concentration does not affect the emulsion viscosity. This has been observed at different water content in the range [3.5-18% vol.]. Thomas law (Thomas, 1965) gives a good interpolation for experimental viscosities as a function of the water

$$\frac{\mu}{\mu_0} = 1 + 2.5\phi + 10.05\phi^2 + 0.00273e^{16.6\phi} \qquad [7]$$

***characterization during crystallisation***

The precise description of crystallisation is performed from the presentation of two types of graphs. The first ones show the evolution of **(**$Q,\Delta P$*)* and second ones show the time evolution of viscosity and water conversion.

Figure 6 presents the influence of additive concentration on **(**$Q,\Delta P$*)* evolution for a water content of 7%. At high high concentration (0.10 %), **(**$Q,\Delta P$*)* remains constant (noted **(**$Q_0,\Delta P_0$**)**) during the overall crystallisation : the viscosity is not modified as the water converts into hydrate. For smaller additive concentrations, we can see that **(**$Q,\Delta P$*)* point starts from **(**$Q_0,\Delta P_0$) and then moves towards to the origin. This means that the gas injection rate is decreased independently of the operator whereas the viscosity remains globally constant, in the range [2.5-3.5 mPa.s]. This effect can be attributed to a blockage, or a plugging at the level of the gas injector.

Figure 7 shows the influence of the water content at a constant additive concentration of 0.10 %. As above mentioned, this concentration is enough to stabilise the emulsion at water content of 7% and to maintain a constant viscosity during crystallisation. This effect is

conserved for a water content of 10%. For water content of 13% and 16%, the **(***Q,ΔP)* evolution is different. Firstly an increase of the viscosity at constant gas injection rate $Q_G$=200-240 l/h is observed. Secondly a decrease of the gas injection at constant viscosity is observed. And finally, the experimental point **(***Q,ΔP)* stabilizes. So, crystallization results in a double effect : fluid viscosity is increased, and gas injector is partially plugged after a while.

The time during which viscosity increases and gas injection rate maintains constant is presented in Figures (8,9). Figure (8) shows that viscosity of 7 % water emulsion remains constant during all the experiment while viscosity of 10 % water emulsion increases slightly to reach a constant value.

At water content of 13% and 16%, the behaviour is similar. Firstly the viscosity increases strongly to reach a maximum. Then, it decreases to reach a constant value. Finally, the viscosity increases again. In Figure (8), the last viscosity increase corresponds to the moment at which the gas injection rate begins to decrease.

At water content of 18%, the viscosity increases rapidly but the flow stops suddenly due to a plug formation.

Figure (9) shows the time evolution of the conversion. There is no clear relation between the water content and the kinetics of gas absorption during crystallisation. It can be noted that the maximum conversion is 50%. Surely, due to the hydrate formation, the left liquid water in the hydrate particles becomes inaccessible to methane and the crystallisation stops.

**Modelling of emulsion crystallization and time evolution of suspension rheology.**

The following work is an attempt to quantitatively interpret the experimental results expressed as $\mu = f\left(t, \phi_{H_2O}\right)$ (figure 8) and $x = f\left(t, \phi_{H_2O}\right)$ (figure 9, $x$ : conversion).

***Conversion evolution***

After the initial absorption, the pressure decrease corresponds to methane consumption by crystallization (Figure 8). The total quantity of consumed gas increases with the water content $\phi_{H_2O}$. The conversion which is not dependent on $\phi_{H_2O}$ ($x < 0.35$) is a quasi-linear function of time. The consumption of methane takes place in the slugs. A mass balance for methane in a slug unit, consisting in a Taylor bubble (TB) and liquid slug, can be written :

$$V_{SL}\left(1-\phi_{H_2O}\right)\frac{dc}{dt} = \left(k_L A\right)_{TB}\left(HP - c\right) - V_{SL}\left(k_L a\right)_{droplets}\left(c - c_{eq}\right) \qquad [8]$$

$c$ : methane concentration in dodecane phase

$c_{eq}$ : methane concentration in dodecane at gas hydrate/liquid water equilibrium

$V_{SL}$ : liquid volume in a slug unit

$k_L$ : mass transfer coefficient

$A$ : area of the Taylor bubble

$a$ : specific surface of water droplets

assuming steady state *dc/dt=0* gives :

$$c = \frac{\left(k_L A\right)_{TB} HP + V_{SL}\left(k_L a\right)_{droplets} c_{eq}}{\left(k_L A\right)_{TB} + V_{SL}\left(k_L a\right)_{droplets}} \qquad [9]$$

and

$$V_{consumption} = \frac{\left(k_L A\right)_{TB} V_{SL}\left(k_L a\right)_{droplets}}{\left(k_L A\right)_{TB} + V_{SL}\left(k_L a\right)_{droplets}}\left(HP - c_{eq}\right) \qquad [10]$$

if $\left(k_L A\right)_{TB} >> V_{SL}\left(k_L a\right)_{droplets}$ then

$$V_{consumption} = V_{SL}\left(k_L a\right)_{droplets}\left(HP - c_{eq}\right) \qquad [11]$$

As the droplet diameter is approximately not dependent on $\phi_{H_2O}$, the volume area of water droplets is proportional to $\phi_{H_2O}$. Then, we can write :

$$V_{consumption} \propto \phi_{H_2O}\left(HP - c_{eq}\right) \text{ or } \quad x \propto \left(HP - c_{eq}\right)t \qquad [12]$$

This equation, which express the experimental results, is based on the following hypothesis : the mass transfer in the vicinity of water droplets and within them is the rate determining step for methane consumption.

***Dynamic viscosity evolution***

After an increase, the dynamic viscosity reaches a plateau. This one is short in the case of high water content. Dynamic viscosity evolution is very sensitive to the water content value. Dynamic viscosity keeps a constant value for $\phi_{H_2O} = 0.07$ whereas it strongly increases with time for $\phi_{H_2O} = 0.18$.

In the case of $\phi_{H_2O} = 0.07$, dynamic viscosity is constant while the conversion in methane hydrate occurs. We can conclude that crystallization, or equivalently conversion of water droplets into crystals, does not modify the dynamic viscosity. Its increase for higher water content values can be explained by agglomeration : agglomerates, which are probably porous, occupy a larger volume than the corresponding dispersed suspension ; as the dynamic viscosity increases with the volume fraction in discrete phase, agglomeration leads to an increase in dynamic viscosity.

Agglomeration in a laminar flow is due to particle encounters which result themselves from velocity gradients thus shear. Generally, agglomeration can be represented by a quasi-chemical reaction between two agglomerates consisting respectively of i and j primary particles :

$$(i) + (j) \rightarrow (i + j)$$

with

$$\frac{dN_{i+j}}{dt} = K_{i,j} N_i N_j \qquad [13]$$

$N_i$ is the number concentration of agglomerate consisting in *i* primary particles.

Kinetic constant ($K_{i,j}$ agglomeration kernel) can be expressed as (Elimelech, 1995):

$$K_{i,j} = \frac{4}{3}\dot{\gamma}\left(R_i + R_j\right)^3 \qquad [14]$$

where $\dot{\gamma}$ is the shear rate, the mean value of which is in a duct :

$$\dot{\gamma} = \frac{16}{3}\frac{U_L}{D} \qquad [15]$$

$U_L$ is the liquid superficial velocity in the duct.

Then, one deduces the characteristic time of agglomeration :

$$\tau = \left(\overline{K}.\overline{N}\right)^{-1} = \left(\frac{64}{9}\frac{U_L}{D}8\overline{R}^3\overline{N}\right)^{-1} = \frac{3\pi}{128}\frac{D}{U_L\phi_{H_2O}} \qquad [16]$$

so, for $U_L = 0.5ms^{-1}$, $D = 0.0102m$, $\phi_{H_2O} = 0.1$, the agglomeration characteristic time is equal to about 0.015s, which we have to compare to the experiment duration (3h). Thus classical agglomeration is very fast. In fact we have to take into account the agglomeration efficiency $\alpha_{i,j}$ (Elimelech, 1995):

$$K_{i,j} = \frac{4}{3}\dot{\gamma}\left(R_i + R_j\right)^3 \alpha_{i,j} \qquad [17]$$

Agglomeration efficiency contains different contributions (Gruy, 2001) : hydrodynamic resistance (leading to a weakly repulsive interaction), physico-chemical forces (attractive Van der Waals interaction) and adsorbed polymer effect. Only the presence of certain additive can lead to an agglomeration efficiency value close to 0. Indeed, this is observed for experiments with $\phi_{H_2O} = 0.07$, but agglomeration for suspension with $\phi_{H_2O} > 0.07$ occurs thanks to another mechanism.

The average distance between surfaces of two drops (made dimensionless by dividing by the drop diameter) of the emulsion checks the expression :

$$\varepsilon = \left( \frac{\pi}{6\phi_{H_2O}} \right)^{1/3} - 1 \qquad [18]$$

This spacing allows the passage of a third drop if :

$$\varepsilon > 1 \qquad \text{or} \qquad \phi_{H_2O} < \frac{\pi}{48} = 0.066 \qquad [19]$$

It is thus understood that the crystallized drops are in a great proximity when $\phi_{H_2O} > 0.07$. The agglomeration must benefit from it. The characteristics of the flow seem secondary compared to the geometrical characteristics of the suspension.

Thus, we suggest the following mechanism :

Three populations coexist in the suspension :

- water drops (index 0),
- crystallized water drops called primary particles (index 1)
- agglomerates with i primary particles

Number concentrations are respectively denoted $N_0, N_1, N_i$

The primary particles are formed in the low temperature (-20°C) derivation loop : the formation rate is proportional to the number concentration in drop :

$$\frac{dN_1}{dt} = k_G N_0 \qquad [20]$$

The formation includes at the same time nucleation and growth of crystals in the drop. The result is a sufficiently solid crystallized drop. These crystallized drops are then transported along the loop of circulation.

The crystallized drops agglomerate by the following mechanism. Let us consider two agglomerates respectively containing *i* and *j* primary particles. Their agglomeration will be done by the intermediary of a not yet crystallized drop. This is represented by the following quasi-chemical equation :

$$(i)+(0)+(j)\rightarrow(i+j+1)$$

The result is an agglomerate with *i+j+1* crystallized primary particles, including the drop (0). This mechanism requires a favoured ternary collision by the already evoked proximity of the drops or particles ($\phi_{H_2O}>0.07$). It explains the strong sensitivity of the agglomeration to water content. It associates the size limits reached by agglomerates to an impoverishment in drops (0). One can also expect the formation of very porous agglomerates because the bonds are done by lonely drops (0).

The conversion of water into gas hydrate occurs parallel to agglomeration. So, methane consumption appears during :

- the transformation of water drops into partially crystallized drops
- the internal growth of partially crystallized drops
- the completion of crystallization in agglomerates

so, methane consumption goes on whereas agglomeration stops because of lack of water drops.

In order to simplify the equation setting, we modify the attribution of an index to an agglomerate. Previously, the agglomerates were identified by their number of primary particles. In fact, one notes that the above-mentioned quasi chemical reaction leads to agglomerates containing *j* initially crystallized drops and *j*-1 initially non crystallized drops :

$$(1)+(0)+(1)\rightarrow(1-0-1)\rightarrow(1-1-1)\equiv(3)$$

$$(1-1-1)+(0)+(1)\rightarrow(1-1-1-0-1)\rightarrow(1-1-1-1-1)\equiv(5)$$

……

Then, the agglomerates contain an odd number of primary particles. One characterizes an agglomerate with $i = 2j - 1$ primary particles by the integer *j*.

So, Three populations coexist in the suspension :

- water drops (index 0),
- crystallized water drops called primary particles (index 1)
- agglomerates with i primary particles (index *j* with $i = 2j - 1$ and $j \geq 2$) .

The population balance can be written (the agglomeration kernel $k_{agg}$ will be kept constant, even if its dependence (unknown) with $\varepsilon$ is strong around $\phi_{H_2O}$=0.07 ):

$$\frac{dN_1}{dt} = k_G N_0 - k_{agg} N_0 N_1 \sum_{j=1}^{\infty} N_j \qquad [21a]$$

$$\frac{dN_k}{dt} = \frac{1}{2} k_{agg} N_0 \sum_{i=1, i+j=k}^{k-1} N_i N_j - k_{agg} N_0 N_k \sum_{j=1}^{\infty} N_j \qquad k > 1 \qquad [21b]$$

The total number of elementary entities (initial concentration of water drops) is constant :

$$N_0 + N_1 + \sum_{k=2}^{\infty} (2k-1) N_k = N_0^0 \qquad [22]$$

where $N_0^0$ is the drop concentration before crystallization (proportional to $\phi_{H_2O}$).

One can make dimensionless this equations set by means of new variables :

$N_k' = \frac{N_k}{N_0^0}$ and $t' = tk_G$

New equation systems is as follows (the previous were removed to make more readable this equations):

$$\frac{dN_1}{dt} = N_0 - k_{agg}^* \phi_{H_2O}^2 N_0 N_1 \sum_{j=1}^{\infty} N_j \qquad [23a]$$

$$\frac{dN_k}{dt} = \frac{1}{2} k_{agg}^* \phi_{H_2O}^2 N_0 \sum_{i=1, i+j=k}^{k-1} N_i N_j - k_{agg}^* \phi_{H_2O}^2 N_0 N_k \sum_{j=1}^{\infty} N_j \qquad [23b]$$

$$N_0 + N_1 + \sum_{k=2}^{\infty} (2k-1) N_k = 1 \qquad [24]$$

The dimensionless agglomeration kernel $k^*_{agg}$ is the new kernel corresponding to the dimensionless equations.

Initial conditions are :

$$t = 0 \quad N_0 = 1 \quad N_k = 0 \quad k > 0 \qquad [25]$$

Numerical solutions are obtained by classical ordinary differential equations solver for $1 < k < 3000$. $k_{agg}$ is a fitting parameter. It is taken independent of $\phi_{H_2O}$.

The dynamic viscosity is obtained from the expression (following Mills, 1985) :

$$\frac{\mu}{\mu_0} = \frac{1-\phi}{\left(1-\frac{\phi}{\phi_{\max}}\right)^2} \qquad [26]$$

$\mu_0, \phi$ are respectively the dynamic viscosity of the continuous phase and the volume fraction in dispersed phase. $\phi_{\max}$ is the volume fraction corresponding to close packing, the value of which is taken equal to 4/7.

For the emulsion :

$$\frac{\mu_e}{\mu_0} = \frac{1-\phi_{H_2O}}{\left(1-\frac{\phi_{H_2O}}{\phi_{\max}}\right)^2} \qquad [27]$$

For the suspension during crystallisation :

$$\frac{\mu_s}{\mu_0} = \frac{1-\phi_{eff}}{\left(1-\frac{\phi_{eff}}{\phi_{\max}}\right)^2} \qquad [28]$$

$\phi_{eff}$ is the effective volume fraction in dispersed phase. It takes into account the compactness or porosity of agglomerates.

As we are only interested by the effect of crystallisation on the suspension dynamic viscosity, we calculate the ratio $\frac{\mu_s}{\mu_e}$.

Following Mills, the effective volume fraction contains contributions of all the agglomerates. We assume that they have a fractal morphology ($D_f$ : fractal dimension). Their outer radius satisfies the equation :

$$\frac{R_i}{R_1} = \left(\frac{i}{S}\right)^{\frac{1}{Df}} \qquad [29]$$

The structure factor *S* is deduced from Gmachowski (1996):

$$S = 0.42 D_f - 0.22 \qquad [30]$$

then, the effective volume fraction can be written ($i = 2k - 1$) :

$$\phi_{eff} = \phi_{H_2O}\left( N_0 + N_1 + \sum_{k=2}^{\infty}\left(\frac{2k-1}{S}\right)^{\frac{3}{Df}} N_k \right) \qquad [31]$$

The above dimensionless concentrations are derived from the numerical solving of the previous system [equations 23-25]. So, we can draw $\frac{\mu_s}{\mu_e} = f\left(t, \phi_{H_2O}\right)$ with 3 fitting parameters $k^*_{agg}$, $k_G$ et $D_f$. $k_G$ is directly related to the time scale.

A sensitivity study of equations system [23-25,27,28,31] to the other parameters $k^*_{agg}$ et $D_f$ shows that they have a strong effect on relative viscosity value at the plateau (Figure 8) and a little effect on the time to reach the plateau. Higher the fractal dimension or lower $k^*_{agg}$, lower the relative viscosity value at the plateau. Optimisation (by a least square method) on $\frac{\mu_s}{\mu_e} = f\left(t, \phi_{H_2O}\right)$ data based on minimization of the standard deviation value $\sigma$ leads to the results presented in Table 1. Parameter $\sigma$ is defined by :

$$\sigma = \frac{1}{n_{H2O}} \sum_{i=1}^{n_{H2O}} \left( \frac{\mu_{r,\exp,i} - \mu_{r,th,i}}{\mu_{r,\exp,i}} \right)^2$$

$n_{H2O}$ is the number (=5) of case studies ($\phi_{H_2O}$ =0.07, 0.10, 0.13, 0.16, 0.18)

This shows (Table 1) that the fractal dimension is probably smaller than 2. In this case the curves have a sigmoid-shape, the relative viscosity evolution for $\phi_{H_2O}$ =0.07, 0.10, 0.16, 0.18 are well represented. On the contrary, the relative viscosity evolution for $\phi_{H_2O}$ =0.13 is less representative. The figure (8) compares experiments and modelling with the following parameters set : $k_{agg}^{*}$ =41, $k_G = 3.1410^{-4}\,\mathrm{s}^{-1}$ et $D_f = 1.8$. So, in this range of water content, modelling shows that the suspension at the plateau contains yet 50 mass percent crystallized drops, 49% agglomerates (i=3 and i=5) and 1% agglomerates with i>5.

**Discussion**

Camargo (2002) compares the rheological properties of hydrate suspensions in an asphaltenic crude oil and in a condensate. Two experimental devices are used : a double coaxial cylinders rheometer and a flow loop.

Asphaltenic crude oil is an high viscosity fluid compared to the condensat. Camargo shows that the corresponding hydrate suspensions exhibited shear-thinning behavior and thixotropy which can be interpreted as the result of a weak reversible flocculation process between hydrate particles. His modelling uses the following relations :

- between viscosity and effective volume fraction (Eq. 28)
- between effective volume fraction and agglomerate size (Eq. 29)
- between agglomerate size, shear stress and interaction forces (see Camargo, 2002)

Asphaltene molecules are adsorbed on the surface of hydrates. Then, interaction forces consist of repulsive steric, attractive interchain and bridging forces between asphaltene-covered

surfaces. The agglomerate size is coming from a force balance between cohesion strength and shear stress, which is proportional to the shear rate.

Condensate chosen by Camargo is similar to dodecane. The behaviours of emulsion and suspensions (same ranges of temperature and pressure, rheology studied in a flow loop) are very close (Camargo, 2001) :

- Newtonian behaviour for emulsions and suspensions
- Same decrease of dynamic viscosity with methane pressure (condensat without water)
- Similar effect of water content on dynamic viscosity for emulsions and suspensions

For Camargo, the explanation of the condensate behaviour is different from the one developed for asphaltene crude oil. In the case of condensate, agglomeration occurs during hydrate formation : due to the hydrophilic character of the hydrate surface, it is believed that capillary forces play an important role : there is formation of water bridges between two hydrate particles. Water bridges may be converted into hydrate bridges, resulting in non-reversible agglomeration process. The presence of additive stabilizing the emulsion does not change this behavior. The importance of capillary forces in agglomeration of hydrate particles has been pointed out by Yang *et al.*(2003) by means of simulations by discrete element method.

The qualitative interpretation of Camargo, early suggested by Austvik *et al* (2000), is in total agreement with our experiments and modelling.

Most of agglomerates contain less than 20 primary particles. Agglomeration stops rapidly by lack of liquid drops. In fact, it is not correct to consider small agglomerates as fractal-like. However, it is always possible to define the size of porous agglomerates (Gruy, 2001) by

means of a power law (Eq. 29). The value of the exponent ($D_f$ = 1.8) proves that these small agglomerates are very porous, i.e. with linear or flat shapes. It is remarkable that Yang (2003) also found small agglomerates (i< 20) after shear induced agglomeration in the same range of shear rate (133 $s^{-1}$ for Yang and 188$s^{-1}$ for this work).

**Conclusion**

Rheology of gas hydrate-water in dodecane system was examined during crystallization process in a loop gas-lift reactor. Emulsion and suspension are Newtonian fluids. The determining-rate step for crystallisation seems to be the methane transfer from dodecane to water drops. At the same time viscosity increases before reaching a constant value and finally increases again. This behaviour is strongly dependent on the water content. It can be explained by considering a mechanism based on an irreversible three-particles agglomeration. It allows us to understand the occurrence of the plateau on viscosity-time plots. Primary particles of agglomerates are coming from water drops which react with methane to form gas hydrate –water drops (crystallized drops). Modelling shows that the aggregates are very porous and contain a few primary particles. These conclusions are in agreement with results coming from literature. The final increase of suspension viscosity is probably connected to an accumulation of gas hydrate crystals in the bottom of riser. The duration of the viscosity steadiness is a decreasing function of water content ; it is probably linked to the hydrate crystas mass accumulated in the riser.

**References**

Austvik, T., Xiaoyun, L., Gjertsen, L.H., 2000, Hydrate plug properties : formation and removal of plugs, Annals of the New York Academy of Sciences, Vol. 912, pp. 294-303

Barnea, D., 1990, Effect of bubble shape on pressure drop calculations in vertical slug flow, Intern. J. of Multiphase Flow, Vol. 16, pp. 79-89

Camargo, R., 2001, Propriétés Rhéologiques de suspensions d'hydrate dans des bruts asphalténiques, P.D. Thesis, Université Paris VI, France

Camargo, R., Palermo, T., 2002, Rheological Properties of Hydrate Suspensions in an Asphaltenic Crude Oil, Proceedings of the Fourth International Conference of Gas Hydrates, Yokohama, May 19-23

Elimelech, M., Gregory, J., Jia, X., Willimas, R., 1995, Particle Deposition and Aggregation, Butterworth-Heinemann, Oxford

Gmachovski, L., 1996, Hydrodynamics of aggregated media, J. Coll Interface Sci., Vol. 178, pp. 80-86

Gruy, F., 2001, Formation of small silice aggregates by turbulent aggregation, J. Colloid and Interface Science, Vol. 237, pp. 28-39

Herri, J.M., F. Gruy, J.S. Pic, Cournil, 1999, M., Methane Hydrate Crystallization Mechanism from in-situ Particle Sizing, AIChE. J. 45 (3), pp. 590-602

Hewitt, G.F., Roberts, D.N., 1969, AERE Report M-2159, Harwell

Mills, P., 1985, Non Newtonian behaviour of flocculated suspensions, Journal de Physique – Lettres, Vol. 46, L301-L39

Pic, J.-S., Herri, J.M, Cournil, M., 2001, Experimental influence of kinetic inhibitors on methane hydrate particle size distribution during batch crystallization, Canadian Journal of Chemical Engineering, Vol. 79, pp. 374-383

Scott, D.S., 1963, Advances in Chemical Engineering, Vol. 4, Academic Press

Sloan, E.D., 1998, Clathrate hydrates of natural gases, Marcel dekker, New-York

Sinquin, A., Palermo, T., Peysson, Y., 2004, Rheological and Flow Properties of Gas Hydrate Suspension, Oil & Gas Science Technology – Rev. IFP, Vol. 59, pp. 41-57

Sylvester, N.D., 1987, A mechanistic model for two-phase vertical slug flow in pipes, Transactions of the ASME J. of Energy Resources Technology, Vol. 109, pp. 206-213

Thomas, D.G., 1965, Transport characteristics of suspensions : VII. A note on the viscosity of Newtonian suspensions of uniform spherical particles, Journal of Colloid Science, Vol. 20, pp. 267-277

Yang Sung-Oh, Graham Mustoe, Sloan, A.D., 2003, Simulation of Hydrate Agglomeration by Discrete Element Method, 15th Symposium on Thermophysical Properties, Boulder, USA, June 22-27, 2003

Yun, J., Shen, Z., 2003, Hydrodynamics of an external-loop gas-lift system with restrictions located in the downcomer, Chem. Engng. Sci., Vol. 58, pp. 377-385

Zhang., H.Q., Lu, M.J., Lian, C.G., Zhu, S.L., 1991, The hydrodynamic model for gas liquid slug flow in vertical tube, J. of Chemical Engineering of Chinese Universities, Vol. 5., pp. 102-111

| | | | | | |
|---|---|---|---|---|---|
| $D_f$ | 1.6 | 1.9 | 2.2 | 2.5 | 3 |
| $k_{agg}$ | 15 | 68 | 480 | 12000 | ∞ |
| σ | 0.03 | 0.03 | 0.036 | 0.054 | |

Table 1 : deviation parameter for different ($D_f$, $k_{agg}$)

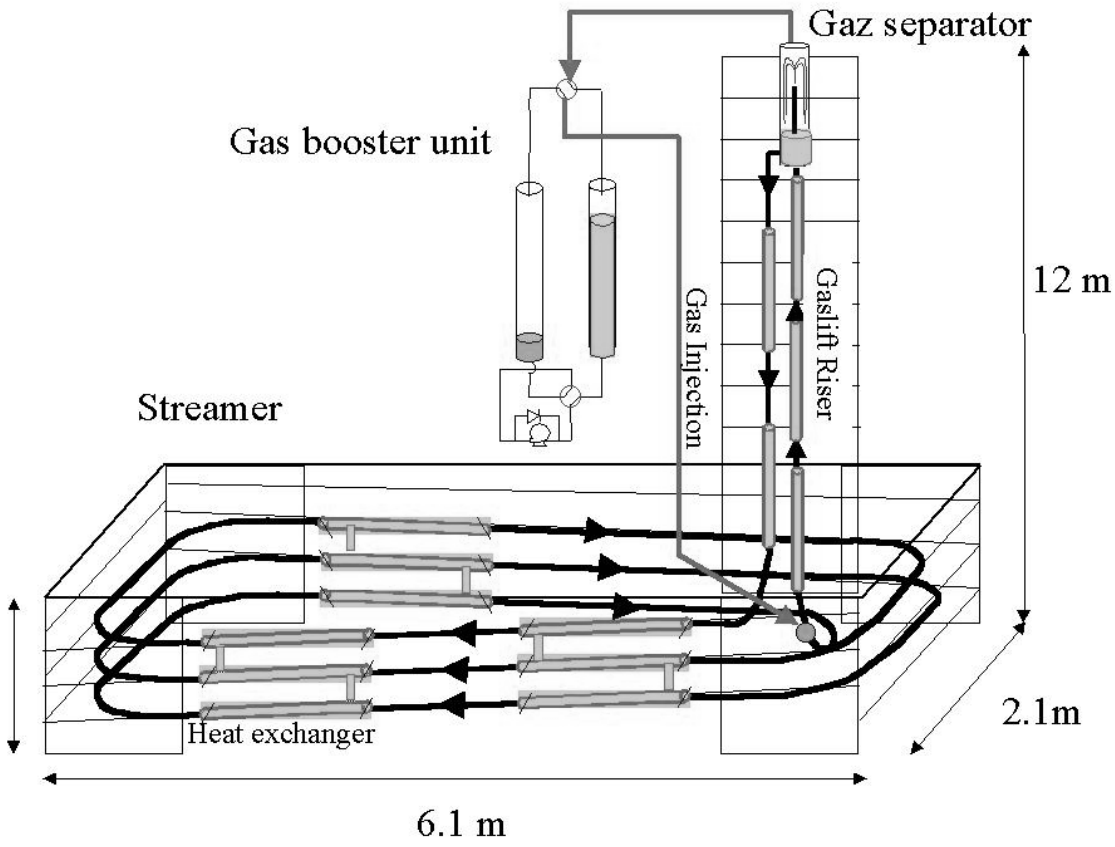


Figure 1
Schematic of the flow loop reactor

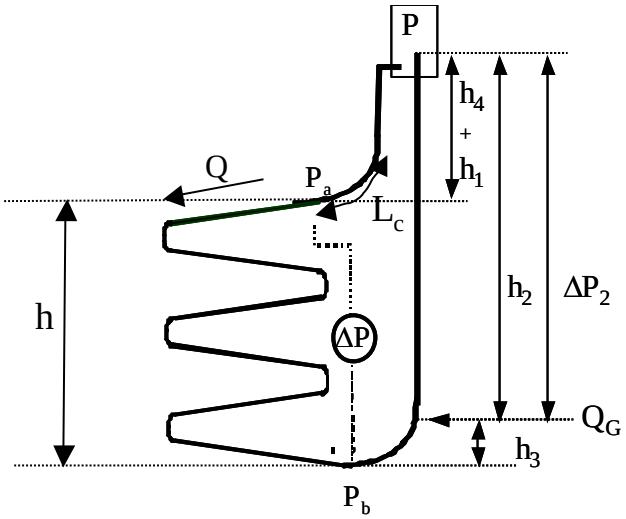


Figure 2
Dimensional elements of the flow loop

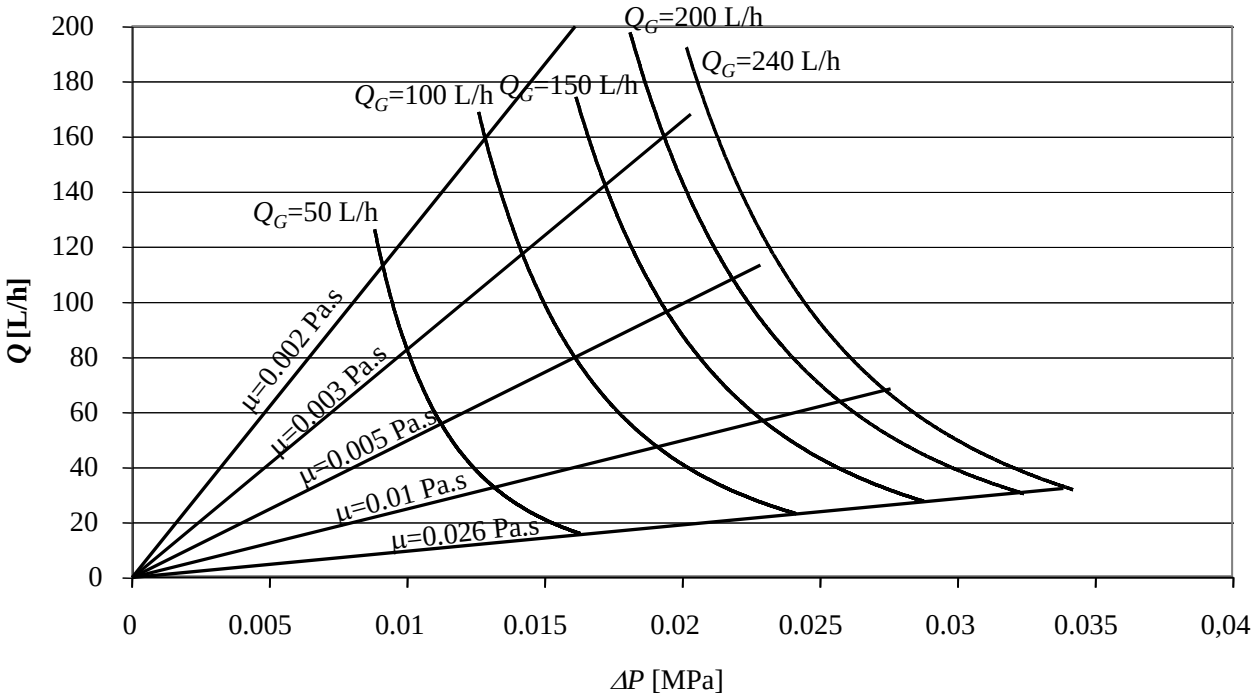


Figure 3
Abacus for $Q = f\left(\Delta P, Q_G\right)$

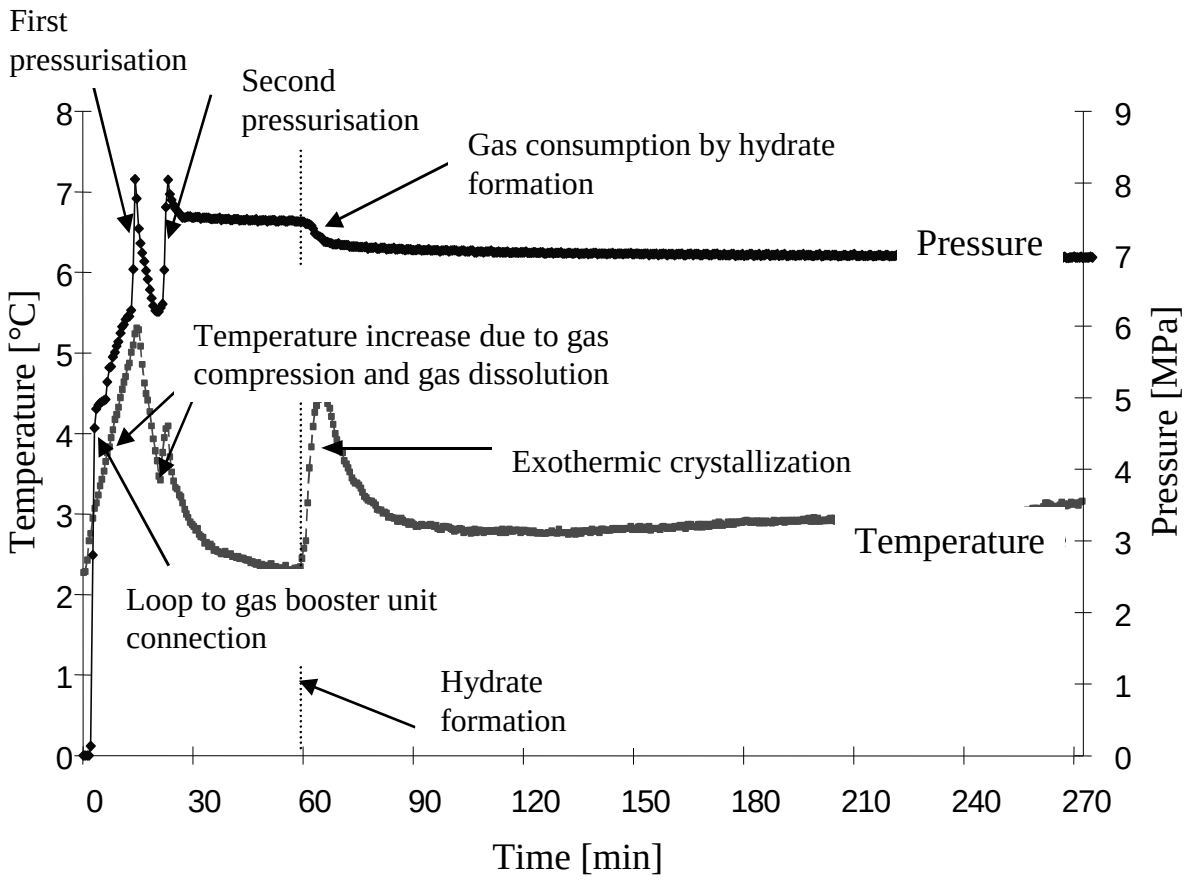


Figure 4
Temperature and pressure in the loop versus time

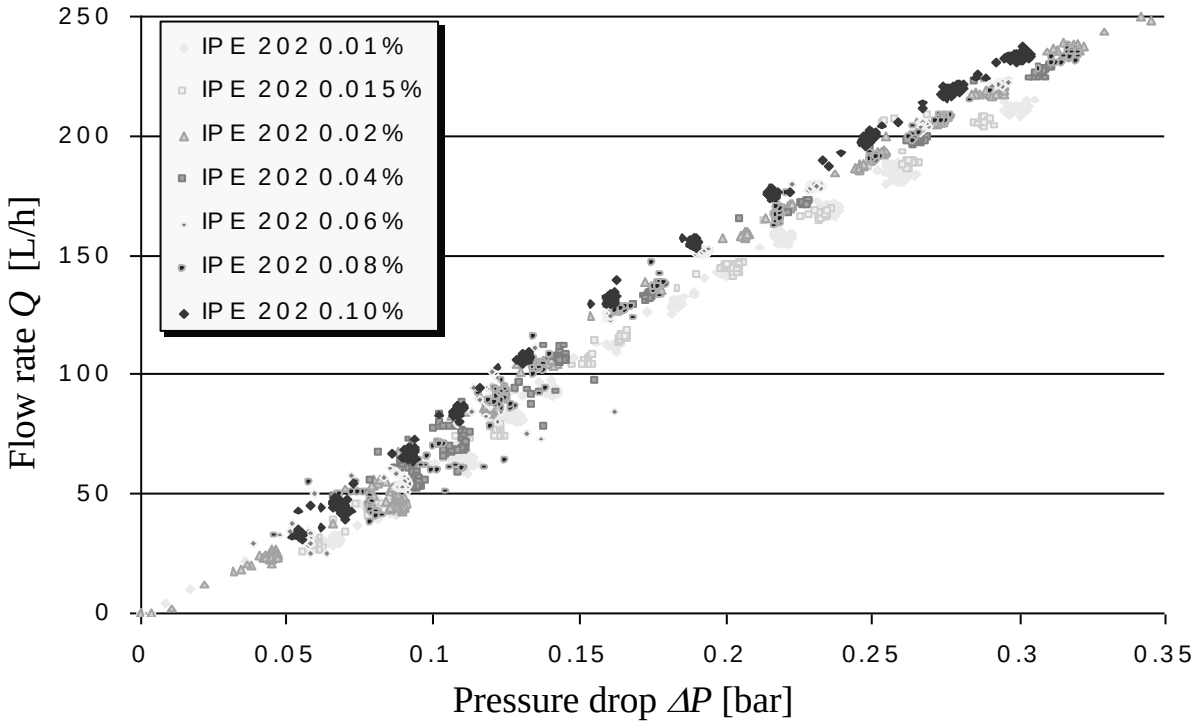


Figure 5
**(***Q,ΔP)* plots for 7% volumic water in dodecane emulsion and influence of IPE 202 additive mass concentration (temperature of 4°C, atmospheric pressure]

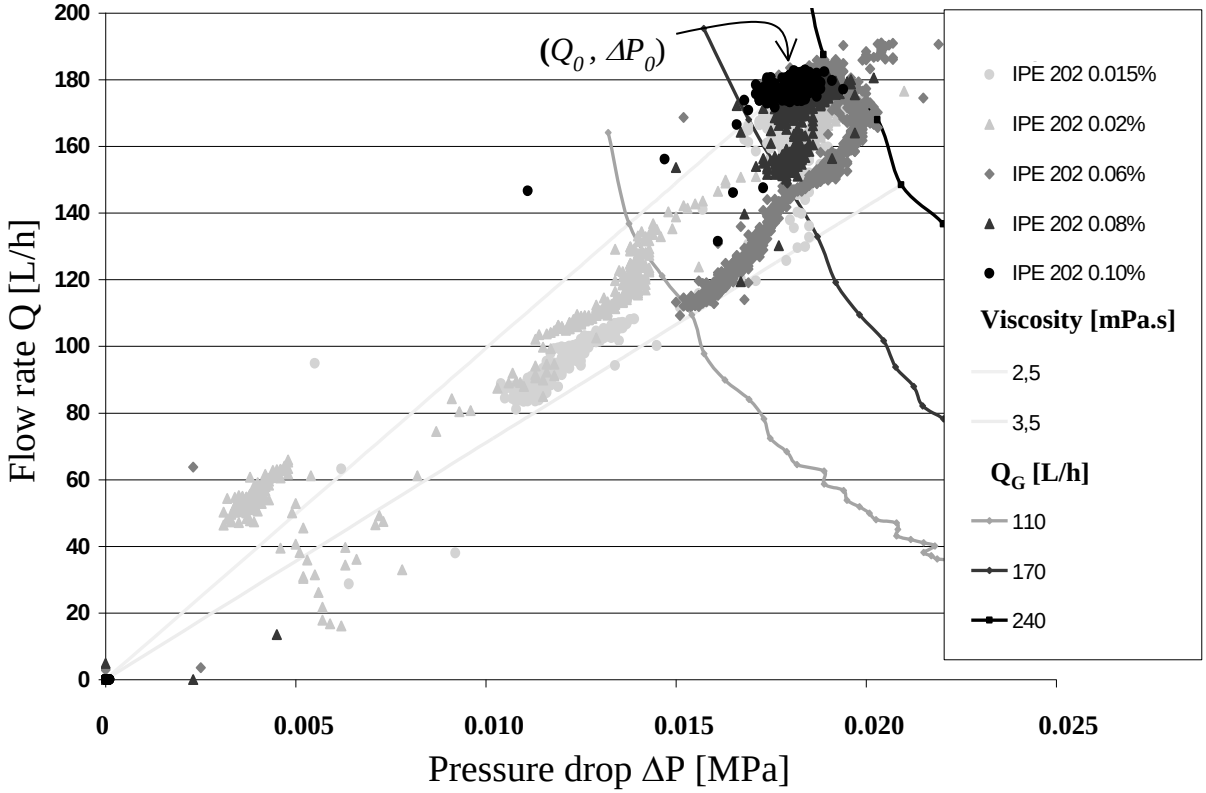


Figure 6
**(***Q,ΔP)* during crystallisation of an 7 % water content emulsion at pressure of 7.5 MPa and temperature of 4°C : influence of additive concentration

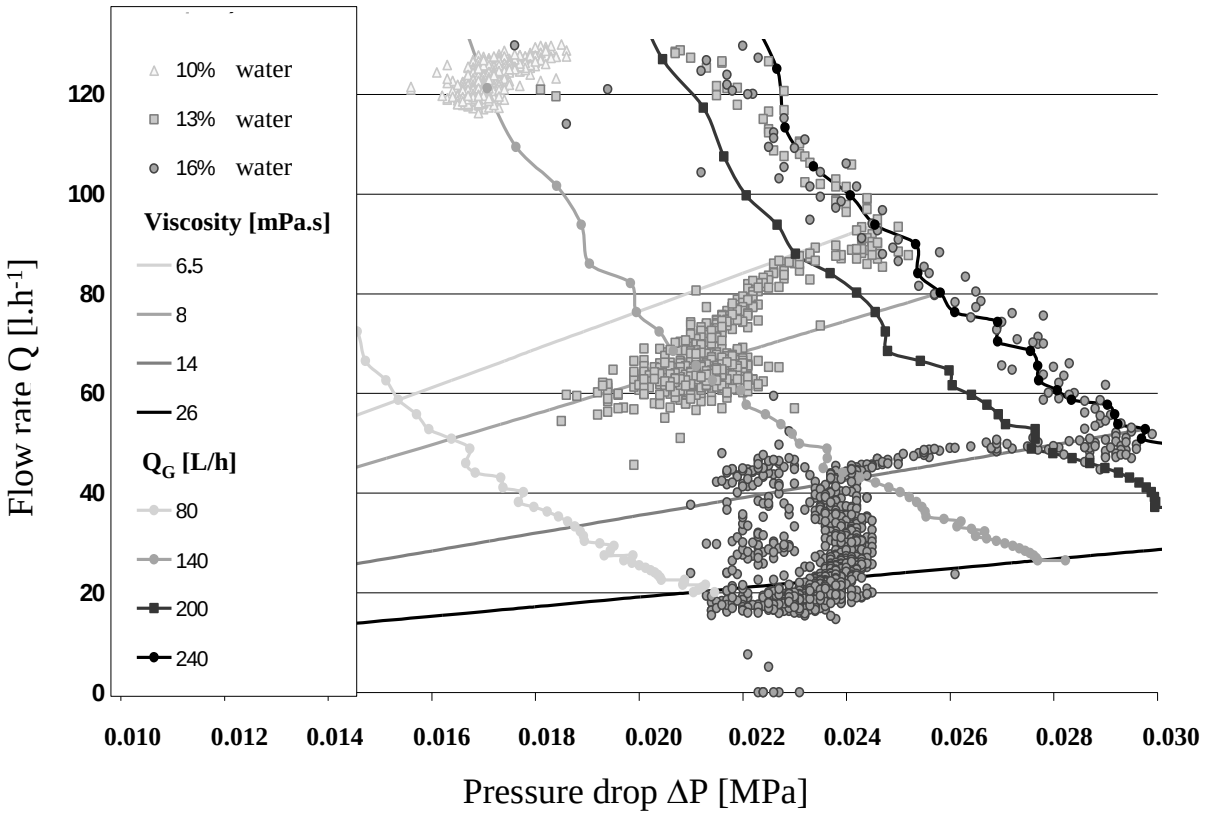


Figure 7
**(***Q,ΔP)* during crystallisation of 10, 13 and 16 % water content emulsions at pressure of 7.5 MPa ,temperature of 4°C and additive concentration of 0.1%

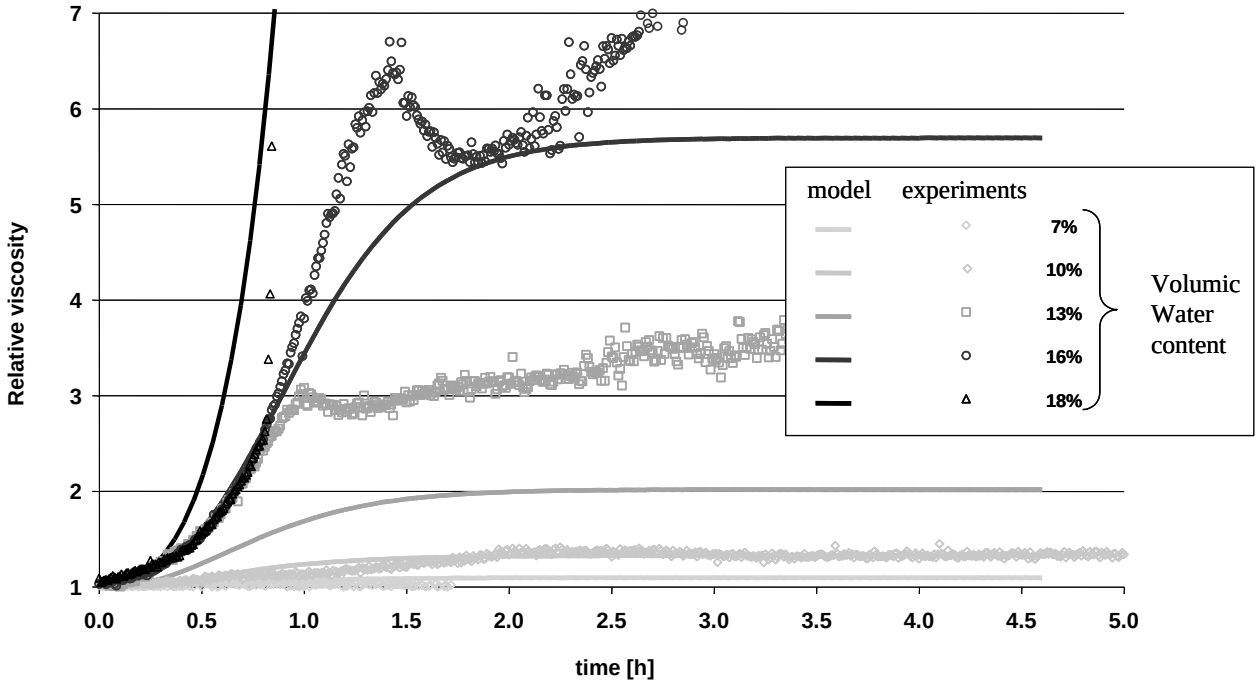


Figure 8
Time evolution of the relative viscosity of hydrate slurries crystallizing in water in oil emulsion at pressure of 7.5 MPa, temperature of 4°C and additive concentration of 0.1% : influence of the water content

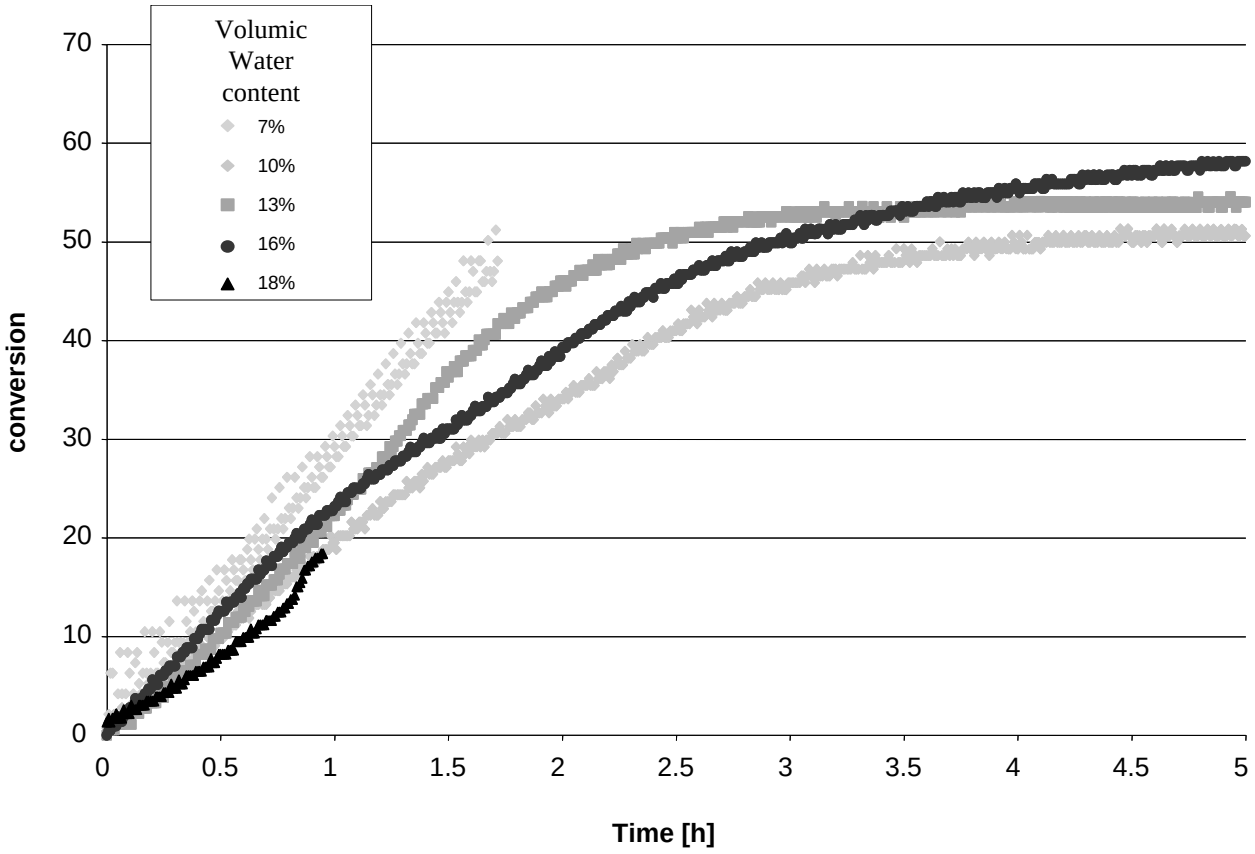


Figure 9
Time evolution of the conversion in hydrate slurries crystallizing in a water in oil emulsion at pressure of 7.5 MPa, temperature of 4°C and additive concentration of 0.1% : influence of the water content

## Notation

| | | |
|---|---|---|
| $A$ | area of the Taylor bubble | $m^2$ |
| $a$ | volume area of water droplets | $m^{-1}$ |
| $c$ | concentration in solute | $mole.m^{-3}$ |
| $c_{eq}$ | concentration in solute at interphase equilibrium | $mole.m^{-3}$ |
| $D$ | internal diameter of the stream section | m |
| $D_1$ | internal diameter of riser and descending pipe | m |
| $D_f$ | fractal dimension | |
| $f$ | friction coefficient | |
| g | acceleration of gravity | $m.s^{-2}$ |
| $k_G$ | kinetic constant of crystallization | $s^{-1}$ |
| $k_{agg}$ | kinetic constant of agglomeration | |
| $k_L$ | mass transfer coefficient | $m.s^{-1}$ |
| $K_{i,j}$ | agglomeration kernel | $m^3.s^{-1}$ |
| $L$ | equivalent rheological length of the stream section (38.5 m) | m |
| $L_i$ | length of section $i$ | m |
| $h_i$ | height of section $i$ | m |
| $N_i$ | number concentration in i-agglomerate | $m^{-3}$ |
| $N_0$ | number concentration in water drop | $m^{-3}$ |
| $N_0^0$ | number concentration in water drop at initial time | $m^{-3}$ |
| $N_i$ | number concentration in i-agglomerate | $m^{-3}$ |
| P | pressure | |
| $Q$ | volumetric flow rate of the flowing phase (without gas phase) | $m^3.s^{-1}$ |
| $Q_G$ | volumetric flow rate of gas in the riser | $m^3.s^{-1}$ |
| $R_i$ | radius of i-agglomerate | m |
| $Re$ | Reynolds Number | |
| $S$ | structure factor of agglomerate | |
| $T$ | temperature | K |
| $t$ | time | s |
| $U_L$ | superficial velocity of liquid | $m.s^{-1}$ |
| $U_G$ | superficial velocity of gas | $m.s^{-1}$ |
| $v$ | flow velocity | $m.s^{-1}$ |
| $V_{SL}$ | liquid volume in a slug unit | $m^3$ |
| $x$ | conversion | $\in[0,1]$ |
| Z | compressibility factor | |

*Greek letters*

| | | |
|---|---|---|
| $\alpha_{i,j}$ | agglomeration efficiency | |
| $\dot{\gamma}$ | shear rate | $s^{-1}$ |
| $\Delta P$ | pressure drop | Pa |
| $\varepsilon$ | average distance between surfaces of two drops | |
| $\mu$ | dynamic viscosity | Pa.s |
| $\mu_e$ | dynamic viscosity of emulsion | Pa.s |
| $\mu_s$ | dynamic viscosity of suspension | Pa.s |
| $\mu_0$ | dynamic viscosity of dodecane | Pa.s |
| $\phi$ | volume fraction in dispersed phase | $\in[0,1]$ |

| | | |
|---|---|---|
| $\phi_{eff}$ | effective volume fraction in dispersed phase | $\in[0,1]$ |
| $\phi_{\max}$ | volume fraction corresponding to close packing | $\in[0,1]$ |
| $\phi_{H_2O}$ | initial volumic water content of the water in oil emulsion | $\in[0,1]$ |
| $\rho$ | mass density of the flowing phase (without gas phase) | $kg.m^{-3}$ |
| $\rho_L$ | mass density of the flowing phase | $kg.m^{-3}$ |
| $\rho_G$ | mass density of the gas phase | $kg.m^{-3}$ |
| $\rho_{GL}$ | mass density of the gas lift | $kg.m^{-3}$ |
| $\sigma$ | deviation | |